ORIGINAL PAPER

Inhibition of CK2 Diminishes Fibrotic Scar Formation and Improves Outcomes After Ischemic Stroke via Reducing BRD4 Phosphorylation

Xuemei Li[1,2] · Qinghuan Yang[1] · Peiran Jiang[1] · Jun Wen[1] · Yue Chen[1] · Jiagui Huang[1] · Mingfen Tian[1] · Jiangxia Ren[1] · Qin Yang[1]

Abstract

Fibrotic scars play important roles in tissue reconstruction and functional recovery in the late stage of nervous system injury. However, the mechanisms underlying fibrotic scar formation and regulation remain unclear. Casein kinase II (CK2) is a protein kinase that regulates a variety of cellular functions through the phosphorylation of proteins, including bromodomain-containing protein 4 (BRD4). CK2 and BRD4 participate in fibrosis formation in a variety of tissues. However, whether CK2 affects fibrotic scar formation remains unclear, as do the mechanisms of signal regulation after cerebral ischemic injury. In this study, we assessed whether CK2 could modulate fibrotic scar formation after cerebral ischemic injury through BRD4. Primary meningeal fibroblasts were isolated from neonatal rats and treated with transforming growth factor-β1 (TGF-β1), SB431542 (a TGF-β1 receptor kinase inhibitor) or TBB (a highly potent CK2 inhibitor). Adult SD rats were intraperitoneally injected with TBB to inhibit CK2 after MCAO/R. We found that CK2 expression was increased in vitro in the TGF-β1-induced fibrosis model and in vivo in the MCAO/R injury model. The TGF-β1 receptor kinase inhibitor SB431542 decreased CK2 expression in fibroblasts. The CK2 inhibitor TBB reduced the increases in proliferation, migration and activation of fibroblasts caused by TGF-β1 in vitro, and it inhibited fibrotic scar formation, ameliorated histopathological damage, protected Nissl bodies, decreased infarct volume and alleviated neurological deficits after MCAO/R injury in vivo. Furthermore, CK2 inhibition decreased BRD4 phosphorylation both in vitro and in vivo. The findings of the present study suggested that CK2 may control BRD4 phosphorylation to regulate fibrotic scar formation, to affecting outcomes after ischemic stroke.

Keywords CK2 · p-BRD4 · Fibroblast · Fibrotic scar formation · Cerebral ischemia

Abbreviations

BRD4	Bromodomain-containing protein 4
CK2	Casein kinase II
HE	Hematoxylin–eosin
TRKI	TGF-β receptor kinase inhibitor
TGF-β1	Transforming growth factor-β1
PP2A	Protein phosphatase type 2A
SD	Sprague–Dawley
TNBC	Triple-negative breast cancer
MCAO/R	Middle cerebral artery occlusion/reperfusion
NADPH	Nicotinamide adenine dinucleotide phosphate
BET	Bromodomain and extraterminal domain
ICAM-1	Intercellular cell adhesion molecule-1
α-SMA	α-Smooth muscle actin
p-BRD4	Phosphorylated bromodomain-containing protein 4
DMSO	Dimethyl sulfoxide
TBB	4,5,6,7-Tetrabromobenzotriazole
FN	Fibronectin
EdU	5-Ethynyl-2′-deoxyuridine
ANOVA	One-way analysis of variance
mNSS	Modified neurological severity score

✉ Qin Yang
xyqh200@126.com

1 Department of Neurology, The First Affiliated Hospital of Chongqing Medical University, 1 Youyi Road, Yuzhong District, Chongqing 400016, China

2 Department of Neurology, The Second People's Hospital of Chongqing Banan District, Chongqing, China

Introduction

After nervous system injury, the inflammatory response is activated, new tissue forms and tissue remodeling occurs [1]. Fibrotic scar formation is involved in tissue repair and reconstruction in the late stage of brain injury. Scars in

the CNS include glial and fibrotic scars [1, 2]. Glial scars, located around the injury site, play a role in preventing neuronal degeneration, inhibiting axonal regeneration, and reconstructing the blood−brain barrier [3, 4]. Fibrotic scars, located at the center of the injury, are composed of a variety of cells with different characteristics and origins (such as the meninges and peripheral blood vessels) [5–7]. These cells migrate to the injury site, transform into myofibroblasts, and secrete extracellular matrix components such as collagen, laminin and fibronectin to form fibrotic scars [8–11]. At present, the role of fibrotic scars in tissue repair and remodeling after CNS injury is unclear. A few studies have shown that fibrotic scars prevent synaptogenesis and aggravate neurological deficits during the remodeling period after brain injury [6, 9, 12]. However, recent studies have shown that complete prevention of fibrotic scarring can lead to cavity formation and hinder functional recovery after spinal injury [13]. Therefore, it is important to elucidate the mechanism of fibrotic scar formation after cerebral ischemic injury to improve patient prognosis.

Casein kinase II (CK2), a messenger-independent serine/threonine protein kinase, is widely present in the cytoplasm and nucleus of eukaryotic cells [14]. CK2 comprises two catalytic subunits (α and/or α′) and two regulatory subunits (β), and it phosphorylates a variety of substrates and participates in cell growth, proliferation, apoptosis, carcinogenesis and other processes [15, 16]. 4,5,6,7-Tetrabromobenzotriazole (TBB) is an efficient and selective ATP competitive inhibitor of CK2, which has a smaller hydrophobic pocket adjacent to the ATP/GTP binding site than do the majority of other protein kinases [17]. TBB enters cells readily and appears not to be cytotoxic in the short term, which makes it useful for experiments [18]. Many studies have shown that CK2 regulates the occurrence and development of fibrosis, inflammation, metabolic diseases, nervous system diseases and tumors [19–23]. CK2 phosphorylates a variety of substrates and regulates fibrosis in peripheral tissues, such as the liver, lung, kidney, and skin [14, 24–26]. Moreover, CK2 is widely expressed in the central nervous system, such as in neurons, microglia, and astrocytes, and regulates neuronal survival, glial cell regeneration, synaptic regeneration and remodeling after stroke [27–30]. However, it remains unclear whether and how CK2 affects fibrotic scar formation after cerebral ischemia injury.

Bromodomain-containing protein 4 (BRD4), a member of the bromodomain and extraterminal domain (BET) family, binds to transcription factors and acetylated histones to recruit multiple transcriptional regulators to control inflammation, chromatin assembly, oxidative stress injury, and cell proliferation [31–33]. BRD4 is highly clustered at gene enhancer sites of genes and regulates fibrosis in a variety of tissues and organs [34–39]. CK2 and protein phosphatase type 2A (PP2A) regulate BRD4 phosphorylation

and dephosphorylation, respectively. There are two CK2 phosphorylation sites (NPS and CPS) in the BRD4 domain [40, 41]. CK2 binds to phosphorylation sites to produce phosphorylated BRD4, which binds to acetylated chromatin and specific transcription factors to regulate site-specific gene transcription [40–43]. Our previous results showed that BRD4 participates in fibrotic scar formation after brain injury [44]. However, whether CK2 regulates fibrotic scar formation after cerebral ischemia by phosphorylating BRD4 has not been determined.

Here, we hypothesized that CK2 inhibition could reduce the activation of fibroblasts induced by TGF-β1 and attenuate fibrosis after cerebral ischemic injury by reducing BRD4 phosphorylation. We found that in vitro, CK2 expression was upregulated in a TGF-β1-induced meningeal fibroblast fibrosis model, and in vivo, CK2 expression was upregulated in a middle cerebral artery occlusion/reperfusion (MCAO/R) injury model. Treatment with SB431542, a TGF-β1 receptor kinase inhibitor, decreased CK2 expression in fibroblasts. The highly potent CK2 inhibitor TBB decreased the proliferation, migration and activation of fibroblasts caused by TGF-β1 in vitro, inhibited fibrotic scarring, ameliorated histopathological damage, reduced Nissl body damage and improved neurological function after MCAO/R injury in vivo. Moreover, CK2 inhibition decreased BRD4 phosphorylation both in vitro and in vivo. This study is the first to indicate that CK2 may control BRD4 phosphorylation to regulate fibrotic scar formation and affect outcomes after MCAO/R injury.

Materials and Methods

Reagents

4,5,6,7-Tetrabromobenzotriazole (TBB) (HY-14394), transforming growth factor-β1 (TGF-β1) (HY-P70543) and SB431542 (HY-10431) were obtained from MedChemExpress (USA). Dimethyl sulfoxide (DMSO; D2650) was obtained from Sigma (USA). A rabbit polyclonal anti-BRD4 primary antibody (DF2905) was obtained from Affinity Company (USA). A rabbit polyclonal anti-phospho-BRD4 (Ser492/Ser494) primary antibody (ABE1453) was obtained from Merck Millipore Company (USA). A polyclonal rabbit anti-CK2α primary antibody (GTX107897) was obtained from GeneTex International Corporation (USA). Alexa Fluor 594-conjugated goat anti-mouse (550042) and Alexa Fluor 488-conjugated goat anti-rabbit (550037) secondary antibodies were obtained from Zen Bioscience (Cheng Du, China). Polyclonal mouse anti-α-SMA (α-SMA; 55135-1-AP), rabbit anti-GAPDH (10494-1-AP), polyclonal mouse anti-FN (66042-1-Ig), HRP-conjugated AffiniPure goat anti-mouse (SA00001-1) and goat anti-rabbit IgG

(SA00001-2) antibodies were obtained from Proteintech (Wuhan, China). Monoclonal rabbit anti-CK2β (ab76025) and a Picrosirius red staining kit (ab150681) were obtained from Abcam (USA). The hematoxylin–eosin (HE) staining kit (G1120), 2,3,5-triphenyltetrazolium chloride (TTC) solution (G3005), Nissl staining kit (methyl violet method) (G1432) and 4% paraformaldehyde (P1110) were obtained from Beijing Solarbio Science & Technology (Beijing, China). A 5-ethynyl-2′-deoxyuridine (EdU) cell proliferation kit with Alexa Fluor 488 (C0071S) and a BCA protein assay kit (P0012S) were obtained from Beyotime Biotechnology Company (Shanghai, China). DMEM/F12 (C11330500BT) was obtained from Gibco (USA). The PCR primers used were obtained from Sangon Biotech (Shanghai, China). Fetal bovine serum (FBS; P30-2602) was obtained from PAN-Biotech (Germany).

Experimental Animals

Neonatal (1–2 days old) and adult male (weight, 200–300 g) Sprague–Dawley (SD) rats were purchased from the Department of Animal Experiments, Chongqing Medical University (Chongqing, China). All adult rats were housed in a temperature-controlled room at a humidity of 40–70% and a temperature of 24–26 °C on a 12 h light/dark cycle and provided free access to food and water. This study was approved by the Animal Experimental Committee of Chongqing Medical University (Ethics Committee Code: 2021-560) and complied with relevant laws such as the IMPROVE and ARRIVE guidelines [45, 46]. The number of rats in each group was predetermined based on previously published studies. Furthermore, researchers blinded to the experimental setup evaluated the outcomes.

Cell Culture

Meningeal fibroblasts from neonatal SD rats were isolated and cultured as previously described by Li et al. [44]. Briefly, the meninges were separated and digested into single-cell suspensions with IV collagenase (1 mg/ml). Fibroblasts were cultured in DMEM/F-12 medium supplemented with 1% penicillin/streptomycin and 10% fetal bovine serum and passaged after they reached confluence. Second- to fourth-generation fibroblasts were used for subsequent studies.

MCAO/R Model

Focal cerebral ischemia was induced by middle cerebral artery occlusion/reperfusion (MCAO/R) in adult SD rats via the insertion of filaments into the artery to occlude blood for 120 min, as described by Longa et al. [47]. Rats that underwent the same surgical procedure but without the insertion of fibrous filaments into the lumen were used for comparison. Rats that developed subarachnoid hemorrhage, died, or had no neurological impairment after surgery were not included in the study.

Drug Treatment

The profibrotic factor TGF-β1 (10 ng/ml) [24, 48–50], the TGF-β1 receptor kinase inhibitor SB431542 (20 μM) [51, 52], and the CK2 inhibitor TBB (5 μmol/l) [24, 53] are commonly used for in vitro studies of fibrosis in a variety of tissues. In our previous research, BRD4 protein expression in primary meningeal fibroblasts was significantly upregulated by 10 ng/ml TGF-β1 and downregulated by 20 μM SB431542 in vitro [44, 52]. TBB (2.5 mg/kg/d and 10 mg/kg/d) administered by intraperitoneal injection inhibited fibrosis in a dose-dependent manner in vivo [14, 24].

Therefore cells were incubated in vitro with TGF-β1 (10 ng/ml), SB431542 (20 μM), dimethyl sulfoxide (DMSO) or TBB (5 μmol/l) for 3 days to evaluate the expression of CK2α and CK2β and the activation of fibroblasts. The solvent SB431542, DMSO or TBB was added to the medium 1 h before TGF-β1 treatment.

In vivo, TBB (5 mg/kg/d) was injected intraperitoneally in volumes of 50 μL or less per rat once a day starting on the day after ischemia−reperfusion. CK2 expression and its effects on fibrotic scar formation were evaluated after MCAO/R injury.

Neurological Deficit Score

Neurological deficit scores were evaluated at 1, 7 and 14 days after MCAO/R via the modified neurological severity score (mNSS) [54], Bederson score [55], and Longa score [47] by an independent investigator. The higher the score is, the more severe the neurological deficit.

The mNSS was used for comprehensive assessment of motor, sensory, reflex, and balance functions. A higher mNSS (0 points, normal; 18 points, loss of consciousness or death) indicates more severe neurological deficits.

The Bederson score was used to measure the forelimb flexion of rats suspended 10 cm, as follows: forelimb extension (0 points); forelimb flexion (1 point); decreased resistance to lateral push (2 points); spontaneous rotation (3 points); circling behavior, decreased activity (4 points).

The Longa score was used to evaluate motor function as follows: normal (0 points); limited left limb movement (1 point); paralysis, walking in circles or rear-end collision (2 points); paralysis, falls or rolls, unable to stand (3 points); and no activity or disorder of consciousness (4 points).

RT−PCR Analysis

The mRNA levels of CK2α, CK2α' and CK2β in TGF-β1-treated meningeal fibroblasts were analyzed at 72 h via RT−PCR. Cultured meningeal fibroblasts were washed and collected. Total RNA was extracted from fibroblasts with TRIzol. Table 1 shows the CK2α, CK2α', CK2β and β-actin primer sequences. Quantitative PCR (qPCR) was carried out on a CFX96 Touch Real-Time PCR Detection System (Bio-Rad, Hercules, USA). The $2^{-\Delta\Delta Ct}$ method, in which β-actin was used for normalization, was used to estimate the amount of target mRNA in the samples. All the samples were analyzed in triplicate.

EdU Assay

The proliferation of meningeal fibroblasts was examined with a 5-ethynyl-2'-deoxyuridine (EdU) cell proliferation kit. First, fibroblasts were seeded in 96-well plates and treated as described above. Second, EdU solution was added to each well, and the cells were incubated for 2 h at 37 °C. Then, the cells were fixed in 4% paraformaldehyde for 15 min and subsequently washed with PBS. Afterward, the cells were stained with Click solution for 30 min at room temperature and DAPI for 15 min at 37 °C. The cells were analyzed with a fluorescence microscope (Olympus, Japan). The cell proliferation rate was detected by the ratio of EdU-positive cells to total cells. The experiments were repeated 3 times.

Scratch Wound Assay

Cell migration was measured with a scratch assay. The meningeal fibroblast monolayer was scratched and incubated with different media for 48 h. Three random fields of the scratch at different time points (0 and 48 h) were observed with a microscope, and the percentage of the wound-healed areas was analyzed by ImageJ software. The experiments were repeated 3 times.

TTC Staining

The infarct volumes in the MCAO/R model rats were examined via TTC staining. Rats were euthanized at 7 days after reperfusion ($n = 3$). The brains were chilled at -20 °C for 20 min to slightly harden the tissue. Six 2 mm coronal sections were cut with a brain matrix (model number 68700; RWD Life Science, Shenzheng, China) on ice and stained with 1.0% TTC solution at 37 °C for 30 min. The infarcts generated by MCAO/R were observed in the striatum and the dorsolateral cortex. The striatum was found to be more sensitive to ischemia than the cerebral cortex [56]. The infarct area was white, whereas the normal tissue was stained red. The stained brain sections were imaged with a digital camera. The infarct volumes were quantified by ImageJ software analysis and calculated by the formula: Infarct volume (%) = (contralateral volume—ipsilateral noninfarct volume)/ contralateral volume × 100 [57].

HE Staining

Rat brain samples were embedded into paraffin blocks and serially sectioned into 4 µm coronal sections. Three nonconsecutive brain slices per rat were randomly selected for each subsequent staining.

A hematoxylin–eosin (HE) staining kit was used to assess the histological structure of the brain. Briefly, brain sections were sequentially stained with hematoxylin solution for 5 min and differentiated with ethanol hydrochloride solution for 3 s and eosin solution for 3 min at room temperature. Three randomly selected regions of interest in the ischemic core of the striatum and the cerebral cortex in each brain slice were photographed under a microscope with blinding at a magnification of ×200. Brain damage after MCAO/R was evaluated by observing the ischemic core structures of the striatum and the cerebral cortex, such as the nucleus (purple−blue), cytoplasm and extracellular matrix (pink). All the experiments were repeated 3 times.

Nissl Staining

A Nissl staining kit (with the methyl violet method) was used to assess the Nissl bodies in cerebral ischemia in rats. The brain sections were treated with methyl violet staining solution for 20 min and washed with Nissl differentiation medium for approximately 8 s. Three randomly selected regions of interest in the ischemic core of the striatum and the cerebral cortex in each brain slice were photographed under a microscope at a magnification of ×200. Dark purple−blue indicates Nissl bodies. Normal neurons had large

Table 1 Primers for RT−PCR

Gene name	Sense (5′–3′)	Antisense (3′–5′)
Csnk2α1	CTGGACAAGCTGCTGCGATACG	CTGCCATGCCAGCCGAACTC
Csnk2α2	CTTCTTGACAAGCTCCTGCGGTAC	AGGCTGGGACTGCTCCTTCAC
Csnk2β	CTTCGGCACTGGTTTCCCTCAC	TTGAAGTTGCTGGCGGCTTGG
β-actin	GGCACCCAGCACAATGAAG	CCGATCCACACGGAGTACTTG

cell bodies with abundant cytoplasm and obvious Nissl bodies. Pyknosis or blurring of Nissl bodies suggested neuronal damage. The number of Nissl bodies was calculated as the area ratio of the Nissl bodies to the image. The results of each section were averaged and statistically analyzed with ImageJ software. All the experiments were repeated 3 times.

Sirius Red Staining

The brain sections were incubated with Picrosirius red solution for 60 min at room temperature and washed with an acetic acid solution. Three randomly selected regions of interest in the ischemic core of the striatum and the cerebral cortex in each brain slice were photographed under a microscope at a magnification of ×200. Collagen fibers were stained red with Sirius red solution. The area of collagen fibers was calculated as the percentage of the image area occupied by collagen fibers. The results for each section were averaged and statistically analyzed with ImageJ software. All the experiments were repeated 3 times.

Immunocytochemistry and Immunofluorescence

Fibroblasts were fixed with paraformaldehyde (4%). The brain sections were microwaved to retrieve the antigen. Afterward, the brain sections or cells were blocked with goat serum (10%) and treated with polyclonal rabbit anti-CK2α antibody (1:100), polyclonal mouse anti-α-SMA antibody (1:100), monoclonal rabbit anti-CK2β antibody (1:100), or polyclonal mouse anti-FN antibody (1:100). For negative controls, PBS was used instead of antibody. After being washed with PBS, the sections or cells were incubated with Alexa Fluor 594-conjugated goat anti-mouse IgG (1:100) and/or Alexa Fluor 488-conjugated goat anti-rabbit IgG (1:100) for 1 h at 37 °C. DAPI staining solution was used to stain the cell nuclei. Finally, the cells were observed and photographed under an A1 + R laser confocal microscope (Nikon, Tokyo, Japan). Three random fields of the central infarct area were selected from each slice. All immunocytochemistry and immunofluorescence assays were repeated three times.

Western Blot Analysis

Protein was extracted from cells or brain tissues from the ischemic core according to the manufacturer's instructions. The protein concentrations of the extracts were assessed by a BCA protein assay kit. Equal amounts of protein from different groups were separated via SDS–PAGE and subsequently transferred to PVDF membranes. After blocking with nonfat milk (5%), the PVDF membranes were treated with rabbit anti-p-BRD4 antibody (1:2000), rabbit anti-BRD4 antibody (1:2000), rabbit anti-CK2α antibody (1:1000), rabbit

anti-CK2β antibody (1:1000), mouse anti-α-SMA antibody (1:2000), rabbit anti-GAPDH antibody (1:10,000) or mouse anti-FN antibody (1:4000). Then, the membranes were incubated with HRP-conjugated AffiniPure goat anti-mouse IgG (1:5000) or goat anti-rabbit IgG (1:5000) secondary antibodies for 1 h. A Bio-Rad instrument was used to quantify the protein bands. Fusion software was used for semiquantitative analysis of protein expression. The gray ratio of the target protein to GAPDH was used to normalize the expression level of the target protein. All the samples were analyzed in triplicate.

Statistical Analysis

SPSS 20.0 for Windows was used to perform the statistical analyses. Quantitative data are presented as the means ± standard deviations (SDs). The results were analyzed with Bonferroni's or Tukey's post hoc test after one-way or two-way analysis of variance (ANOVA). Single comparisons were analyzed by Student's t test. Neurological deficit scores are expressed as medians and ranges and were analyzed with the Kruskal−Wallis test followed by Dunn's post hoc test. $P < 0.05$ was considered to indicate statistical significance.

Results

CK2α and CK2β Expression is Increased in a TGF-β1-Induced Fibrosis Model In Vitro and an MCAO/R-Induced Fibrotic Scar Formation Model In Vivo

TGF-β1 is an important contributor to fibrosis. We first investigated whether CK2 expression is altered in a TGF-β1-induced meningeal fibroblast fibrosis model in vitro. RT−PCR analysis revealed that the expression levels of CK2α, CK2α' and CK2β mRNAs in the TGF-β1 and TGF-β1 + DMSO groups were significantly greater than those in the Con and TGF-β1 + SB431542 groups (Fig. 1B–D). In addition, Western blotting analysis showed that the protein expression levels of CK2α and CK2β in the TGF-β1 and TGF-β1 + DMSO groups were significantly greater than those in the Con and SB431542 groups (Fig. 1E–G). The results suggested that CK2 expression was upregulated by TGF-β1 and downregulated by SB431542 in meningeal fibroblasts, which indicated that CK2 may play a role in TGF-β1-induced meningeal fibroblast fibrosis.

Next, we investigated whether fibrotic scar formation and CK2 expression were affected after MCAO/R injury. Immunofluorescence and Western blotting demonstrated that the expression of CK2α, CK2β and fibronectin (FN; a marker of fibrotic scarring) in the infarct core at 7 and
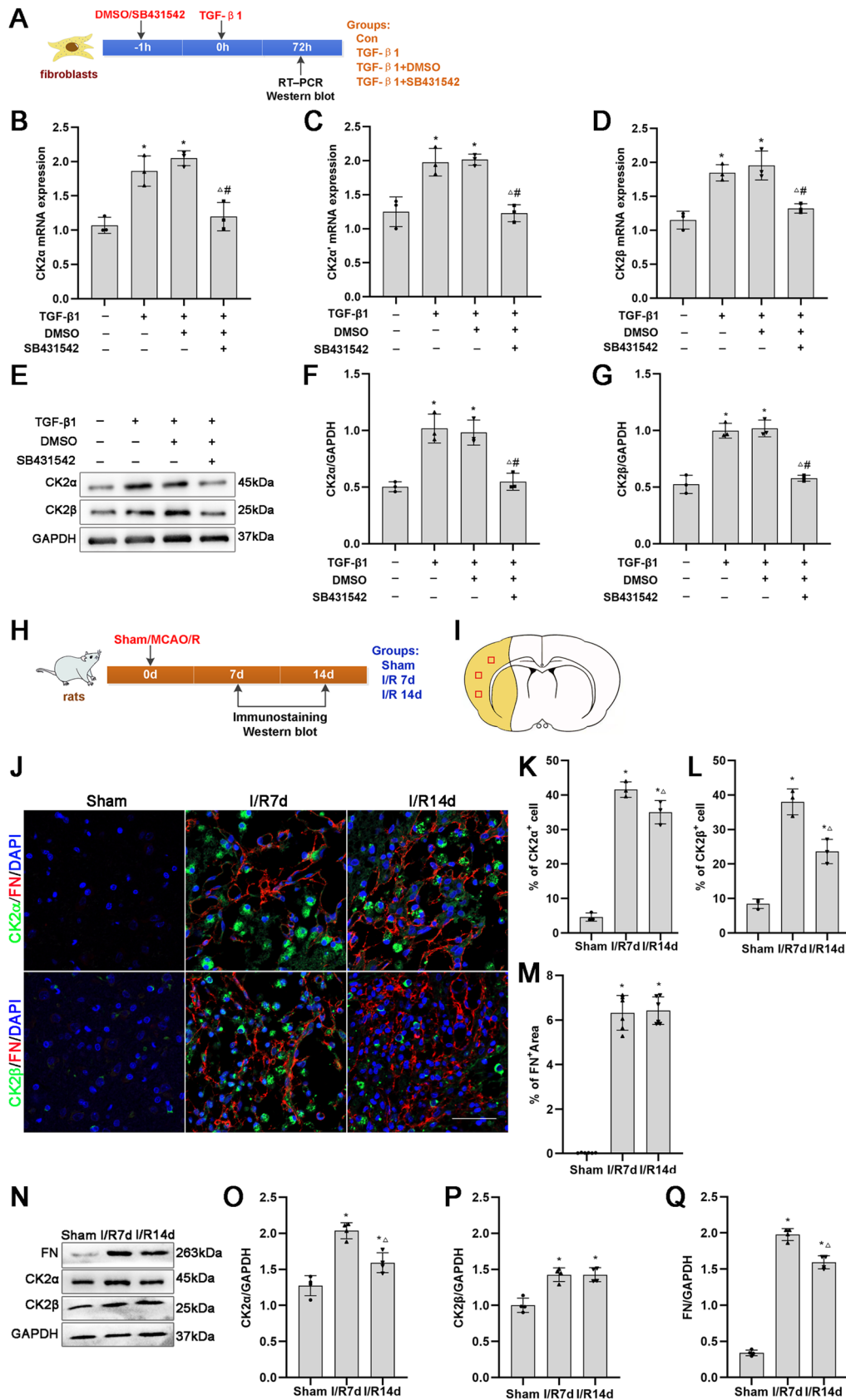
◄**Fig. 1** CK2α and CK2β expression was increased in vitro in the TGF-β1-induced fibrosis model and in vivo in the MCAO/R injury model. **A** Timeline of fibroblast treatment. **B–D** RT−PCR analysis of CK2α, CK2α′ and CK2β mRNA expression in each group of fibroblasts treated with TGF-β1 for 72 h (*n*=3). **E–G** Representative protein expression and quantification data for CK2α and CK2β in each group of fibroblasts were obtained by Western blotting (*n*=3). *$P<0.05$ vs. the Con group; $^{\triangle}P<0.05$ vs. the TGF-β1 group; $^{\#}P<0.05$ vs. the TGF-β1+DMSO group. **H** Timeline and group diagram of the rats. **I** Schematic diagram of the coronal plane of the brain. The ischemic core is represented by the yellow area. The observed regions are shown as square boxes. **J** Immunofluorescence staining of FN$^+$/CK2α$^+$ and FN$^+$/CK2β$^+$ cells and images of merged signals in the ischemic core after cerebral ischemia (*n*=3). Red represents tissue immunostained with antibodies against FN, and green represents cells immunostained with antibodies against CK2α or CK2β. Scale bars: 50 μm. **K–M** Representative quantitative analysis of FN-positive areas and CK2α-positive and CK2β-positive cells. **N–Q** Protein expression and quantification of FN, CK2α and CK2β levels in the ischemic core after cerebral ischemia caused by MCAO/R, as detected by Western blotting (*n*=3). *$P<0.05$ vs. the sham group; $^{\triangle}P<0.05$ vs. the I/R 7 d group

14 days after MCAO/R was significantly greater than that in the sham group (Fig. 1J–Q). Moreover, the protein expression of CK2α and FN in the I/R7d group was significantly greater than that in the I/R14d group (Fig. 1J–Q). These results indicated that cerebral ischemic injury significantly induced fibrosis and upregulated the expression of CK2α and CK2β in the infarct core at 7 days. Therefore, in the subsequent study, observation was performed 7 days after MCAO/R.

Our study showed that the expression of CK2α and CK2β was upregulated in the TGF-β1-induced fibrosis model and MCAO/R injury model.

TBB Inhibits the Proliferation, Migration and Activation of Meningeal Fibroblasts In Vitro

The above findings indicate that CK2 expression was upregulated in fibrosis models both in vitro and in vivo. We further investigated whether CK2 inhibition by TBB, a selective ATP-competitive inhibitor of CK2, affects the proliferation, migration and activation of meningeal fibroblasts caused by TGF-β1 in vitro.

The proliferation, migration and secretion of extracellular matrix from fibroblasts are involved in fibrous scar formation. EdU and scratch wound assays showed that cell proliferation and migration were significantly upregulated in the TGF-β1 and TGF-β1+DMSO groups and downregulated in the TGF-β1+TBB group (Fig. 2B–C, D–E). α-SMA is a marker of fibroblast activation, and FN is an extracellular matrix component secreted by activated fibroblasts. Immunofluorescence analysis demonstrated that α-SMA and FN protein expression was significantly upregulated in the TGF-β1 and TGF-β1+DMSO groups and downregulated in the TGF-β1+TBB group compared with the control

group (Fig. 2F–H). Western blotting analysis also showed that TGF-β1 up-regulated the expression of the α-SMA and FN proteins, and TBB had the opposite effect (Fig. 2I–K).

These results indicated that CK2 could regulate the proliferation, migration and activation of fibroblasts induced by TGF-β1.

TBB Inhibits Fibrosis, Ameliorates Damage, Protects Nissl Bodies, and Improves Outcomes After MCAO/R Injury

TBB inhibited TGF-β1-induced fibroblast activation in vitro. We further investigated whether CK2 inhibition by TBB affects fibrotic scar formation and outcomes after MCAO/R injury in vivo.

Collagen fibers, FN and α-SMA are markers of fibrotic scar formation. Collagen fibers are fibrous components that consist primarily of collagen and amino acids. Under a light microscope, the collagen fibers were stained red with a yellow background by Sirius red staining. Sirius red staining, immunofluorescence and Western blotting revealed significantly more collagen fibers and significantly higher α-SMA and FN protein expression in the infarct core in the Ctrl, vehicle and TBB groups than in the sham group and lower in the TBB group than in the Ctrl and vehicle groups (Fig. 3C–K). These results suggested that TBB inhibited fibrous scar formation in the ischemic core after MCAO/R injury.

Hematoxylin and eosin (H&E) staining was performed to assess histopathological damage after MCAO/R injury. The results showed that the structure of the striatum and the cerebral cortex in the sham group was normal. In these rats, the neurons were densely and evenly arranged, with a normal structure and morphology, clear cell contours, and clearly visible and intact nucleoli. In contrast, the histological structure of the brain was disrupted after MCAO/R injury, with tissue necrosis, neuronal loss and marked glial cell infiltration in the ischemic core. However, the morphological changes in the TBB group were less severe than those in the Ctrl and vehicle groups (Fig. 4C).

Nissl bodies are basophilic masses and granules composed of rough endoplasmic reticulum and free ribosomes in the cell body or dendrites of neurons and are markers of neurons. The Nissl body staining results showed neurons with large cell bodies, abundant cytoplasm and obvious Nissl bodies in the sham group and neurons with pyknosis or blurred Nissl bodies in the Ctrl, vehicle and TBB groups. Moreover, the number of Nissl bodies in the infarct core was significantly lower in the Ctrl and vehicle groups than in the sham group and greater in the TBB group than in the Ctrl and vehicle groups (Fig. 4D, E).

The infarct volume was evaluated via TTC staining to assess brain injury at 7 days after MCAO/R. As shown in
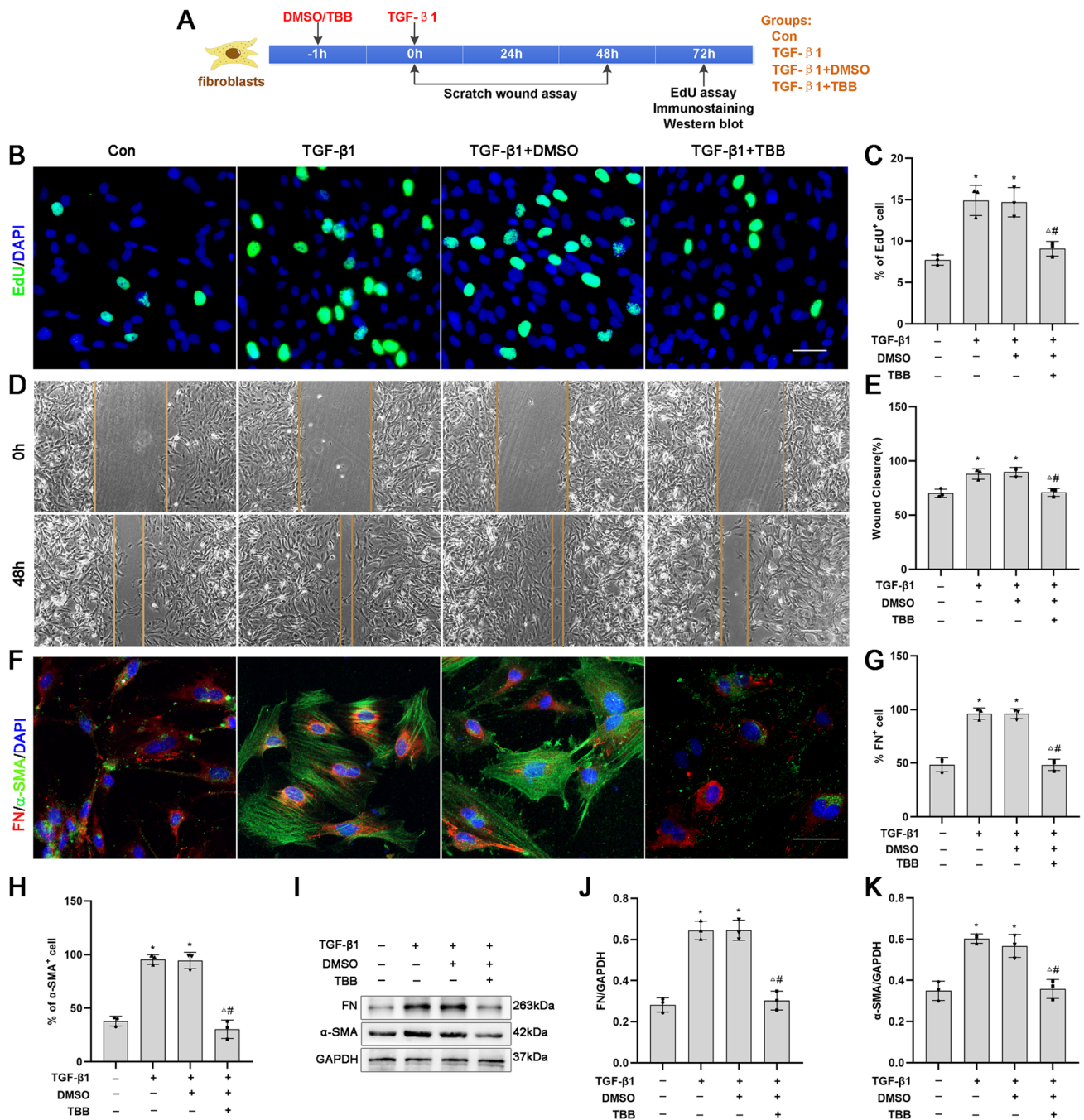
Fig. 2 Effects of TBB on the proliferation, migration and activation of fibroblasts induced by TGF-β1 in vitro. **A** Timeline of fibroblast treatment. **B**, **C** Fibroblast proliferation in each group induced by TGF-β1 for 72 h was detected by EdU analysis. Green and blue represent EdU-positive cells and nuclei, respectively ($n = 3$). Scale bars: 50 μm. **D**, **E** The migration of fibroblasts in each group was detected by the scratch wound assay ($n = 3$). Scale bars: 200 μm. **F**–**H** The activation of fibroblasts in each group was detected by immuno-fluorescence staining with antibodies against α-SMA and FN. Green indicates the α-SMA, and red indicates the FN. ($n = 3$). Scale bars: 50 μm. **I–K** Representative protein expression and quantification analysis of α-SMA and FN protein levels in fibroblasts induced by TGF-β1 for 72 h, as detected by Western blotting ($n = 3$). *$P < 0.05$ vs. the Con group; $^{\triangle}P < 0.05$ vs. the TGF-β1 group; $^{\#}P < 0.05$ vs. the TGF-β1 + DMSO group

Fig. 4F and G, there was no cerebral infarction in the sham group. The infarct volume was significantly lower in the TBB group than in the Ctrl and vehicle groups. The results showed that TBB significantly decreased the infarct volume after MCAO/R.

Neurological deficits in the rats were evaluated with the mNSS, Bederson score, and Longa score at 1, 7 and 14 days
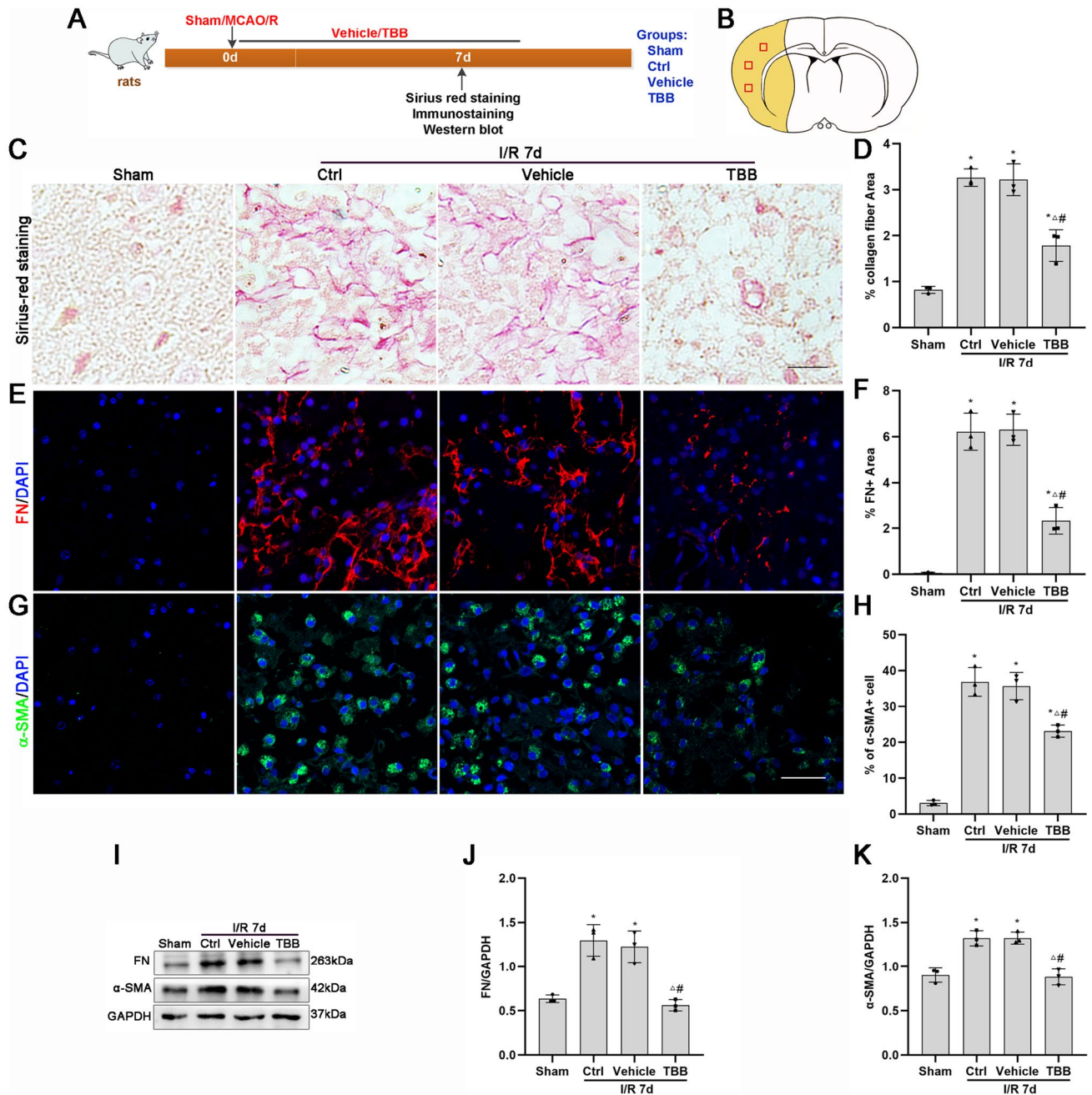
Fig. 3 TBB reduces fibrosis after MCAO/R injury. **A** Timeline and group diagram of the rats. **B** Schematic diagram of the coronal plane of the brain. The ischemic core is represented by the yellow area. The regions of interest are shown as square boxes. **C**, **D** Expression and quantitative analysis of collagen fibers with Sirius red staining at 7 days after MCAO/R ($n=3$). Red represents collagen fibers. Scale bars: 1 μm. **E–H** Protein expression levels and quantitative analysis of FN and α-SMA at 7 days after cerebral ischemic injury determined by immunofluorescence staining ($n=3$). Red represents FN-positive areas. Green represents α-SMA-positive cells. Blue represents nuclei. Scale bars: 40 μm. **I–K** Protein expression levels and quantitative analysis of α-SMA and FN in the ischemic core at 7 days after MCAO/R injury determined by Western blotting ($n=3$). *$P<0.05$ vs. the sham group; $^{\triangle}P<0.05$ vs. the Ctrl group; $^{\#}P<0.05$ vs. the vehicle group

after MCAO/R injury (Fig. 4H–J). There was no neurological deficit in the sham group. The rats in the Ctrl, vehicle and TBB groups exhibited obvious neurological deficits after MCAO/R, which were gradually alleviated over time.

There were significantly fewer neurological deficits in the TBB group than in the Ctrl and vehicle groups at 7 and 14 days, but there was no significant difference at 1 day after MCAO/R. The results showed that neurological deficits after
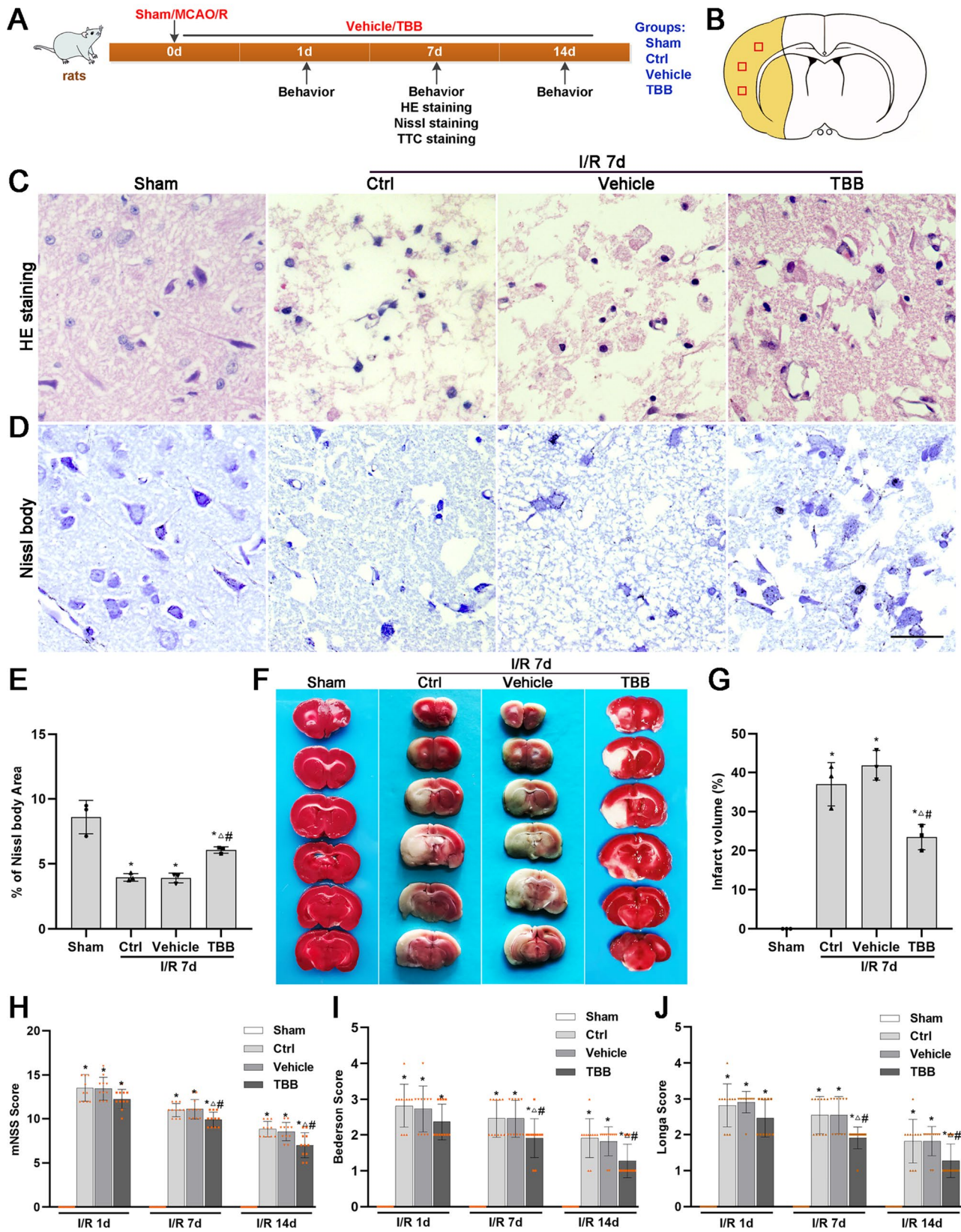
◂**Fig. 4** TBB ameliorates histopathological damage, protects Nissl bodies, decreases infarct volume and ameliorates neurological deficits after MCAO/R injury. **A** Timeline and group diagram of the rats. **B** Schematic diagram of the coronal plane of the brain. The ischemic core is represented by the yellow area. The observed regions are shown as square boxes. **C**, **D** Representative histological structure assessed by HE staining and Nissl body (bluish violet) expression assessed by Nissl staining of the ischemic core at 7 days after MCAO/R injury ($n = 3$). Scale bars: 2 μm. **E** Quantitative analysis of Nissl bodies expressed as the area ratio of the Nissl bodies to the image. **F**, **G** Representative images and quantitative analysis of the infarct volume in brain slices after MCAO/R determined by TTC staining ($n = 3$). White indicates infarction, while red indicates normal tissue. Analysis of neurological function according to the mNSS (**H**), Bederson score (**I**), and Longa score (**J**) at 1, 7 and 14 days after MCAO/R injury ($n = 12$). *$P < 0.05$ vs. the sham group; $^{\triangle}P < 0.05$ vs. the Ctrl group; $^{\#}P < 0.05$ vs. the vehicle group

stroke were gradually alleviated in a time-dependent manner. TBB significantly improved stroke outcomes, with better outcomes observed at 14 days than at 7 days.

These results showed that the CK2 inhibitor TBB decreased fibrotic scar formation, reduced brain damage and Nissl body loss, and improved neurological outcomes after MCAO/R.

TBB Inhibits BRD4 Phosphorylation in a TGF-β1-Induced Fibrosis Model In Vitro and an MCAO/R Injury Model In Vivo

The above studies showed that CK2 is involved in the TGF-β1-induced activation of meningeal fibroblasts in vitro and in fibrotic scar formation after MCAO/R injury in vivo. We further investigated whether CK2 regulates fibrosis by affecting BRD4 phosphorylation.

Western blotting revealed that the protein levels of BRD4 and p-BRD4 were increased in the in vitro TGF-β1-induced fibrosis model and in the in vivo MCAO/R injury model (Fig. 5A–H). The CK2 inhibitor TBB decreased the level of p-BRD4 but not the BRD4 protein in vitro (Fig. 5A–D). Moreover, TBB had a similar effect on the ischemic core after MCAO/R (Fig. 5E–H). These results showed that the CK2 inhibitor TBB reduced BRD4 phosphorylation both in vitro in a TGF-β1-induced fibrosis model and in vivo during MCAO/R injury-induced fibrotic scar formation, which suggested that CK2 regulates fibrosis by phosphorylating BRD4 in vitro and in vivo.

Discussion

The present study showed that CK2 expression was upregulated in vitro in a TGF-β1-induced meningeal fibroblast fibrosis model and in vivo in a middle cerebral artery occlusion (MCAO)/reperfusion (R) injury model. Treatment with SB431542, a TGF-β1 receptor kinase inhibitor, decreased

CK2 expression in fibroblasts. The highly potent CK2 inhibitor TBB decreased the proliferation, migration and activation of fibroblasts caused by TGF-β1 in vitro, inhibited fibrotic scarring, ameliorated histopathological damage, reduced Nissl body damage and improved neurological function after MCAO/R injury in vivo. Moreover, CK2 inhibition decreased BRD4 phosphorylation in vitro and in vivo. This study is the first to indicate that CK2 may control BRD4 phosphorylation to regulate fibrotic scar formation and affect outcomes after MCAO/R injury.

CK2 is a protein kinase that occurs widely in eukaryotic cells and participates in cell growth, proliferation, apoptosis and other processes. CK2 is composed of two catalytic subunits (α and/or α′) and regulatory subunits (β). Several studies suggest that the α catalytic subunit has important kinase activity and is the primary functional subunit for disease treatment [14, 58, 59]. The β subunit is likely responsible for the oncogenic potential of CK2. In epithelial–mesenchymal transition (EMT), TGF-β signaling increases CK2 activity by decreasing the protein level of CK2β without affecting the protein level of CK2α [48]. Many studies have shown CK2 participates in liver, lung, skin and kidney fibrosis [24, 26, 60]. In systemic sclerosis fibroblasts, CK2α and CK2β expression was also increased. Here, we found that CK2α and CK2β expression was upregulated during fibrotic scarring after stroke and in a TGF-β1-induced fibrosis model, respectively. These findings suggest CK2 may participate in the regulation of fibrotic scarring after cerebral ischemia, which is consistent with previous findings.

CK2 regulates tissue fibrosis through a variety of signaling pathways, such as the TGF-β1/Smad3, p-NF-κB [25], Wnt/β-catenin [26], IKK/NF-κB [14], and JAK2/STAT3 pathways [24] and non-Smad signaling pathways (Akt and Erk) [61]. CK2 also controls tissue and cellular functions by phosphorylating a variety of substrates. For example, CK2 regulates BRD4 function by binding to phosphate sites (NPS and CPS) in the BRD4 domain [40]. CK2-mediated BRD4 phosphorylation promotes resistance to BET inhibitors in lung adenocarcinoma, while CK2 inhibitors reduce resistance [62]. In drug-resistant triple-negative breast cancer cells, decreased PP2A activity causes hyperphosphorylation of BRD4 [63]. In addition, the CK2 inhibitor TBB or CK2 knockout reduces neuronal immediate early gene expression and inhibits synaptic remodeling and memory generation by controlling BRD4 phosphorylation [64]. Here, our results showed that CK2 regulates fibrous scar formation after MCAO/R injury by affecting BRD4 phosphorylation. Therefore, CK2 may play multiple roles through multiple signaling pathways or through the phosphorylation of multiple substances in different organs.

CK2 occurs widely in neurons, astrocytes and myelin sheaths and participates in a variety of functions in the central nervous system [27, 28]. For example, CK2 inhibited
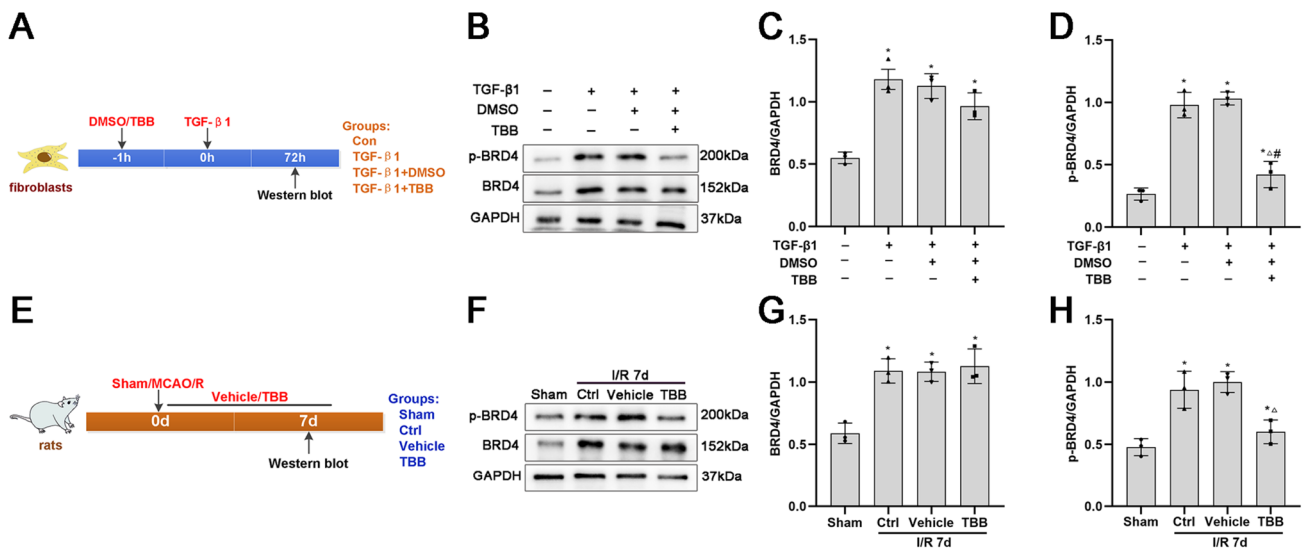
Fig. 5 Effects of TBB on BRD4 phosphorylation in vitro and in vivo. **A** Timeline of fibroblast treatment. **B–D** Representative protein expression and quantitative analysis of p-BRD4 and BRD4 protein levels in fibroblasts incubated with TGF-β1 and/or TBB for 72 h, determined by Western blotting ($n = 3$). *$P < 0.05$ vs. the Con group; $^{\triangle}P < 0.05$ vs. the TGF-β1 group; $^{\#}P < 0.05$ vs. the TGF-β1+DMSO group. **E** Timeline and group diagram of the rats. **F–H** Representative protein expression and quantitative analysis of p-BRD4 and BRD4 protein levels in the ischemic core at 7 days after cerebral ischemia injury, as assessed by Western blotting ($n = 3$). *$P < 0.05$ vs. the sham group; $^{\triangle}P < 0.05$ vs. the Ctrl group; $^{\#}P < 0.05$ vs. the vehicle group

NADPH oxidase-triggered oxidative stress injury and reduced neuronal death 24 h after brain injury [30]. CK2 regulated the activation and migration of microglia induced by ischemia and hypoxia and controlled glial scar formation [65]. CK2 inhibition could promote oligodendrocyte survival, protect axonal structure and axonal mitochondrial function, and improve neurological function after cerebral ischemia [53, 66, 67]. Moreover, CK2 regulates platelet synthesis, activation and thrombosis, and CK2β knockout significantly reduces cerebral infarct volume, alleviates neurological deficits and improves the prognosis in rats with cerebral ischemia [68]. Similarly, our findings showed that CK2 controlled fibroblast activation and fibrosis at 7 days after cerebral infarction. These studies suggest that CK2 plays different or even opposing roles in different tissues.

In addition, the study had several limitations. For example, CK2 is expressed in almost all mammalian cells. We intraperitoneally injected the CK2 inhibitor TBB to detect fibrous scar formation after cerebral infarction in vivo. Whether intraperitoneal TBB acted on other cells, such as platelets, endothelial cells and immune cells, and thereby indirectly affected the repair of cerebral infarction is unknown. Therefore, lateral intraventricular administration of TBB will be used to reduce the effect of TBB on peripheral tissues and cells in future research. In addition, fibrous scar formation after stroke involves a variety of cells, such as meningeal fibroblasts, pericytes and stromal cells. Whether and how these cells interact with each other needs to be further investigated.

Conclusion

Our present data demonstrate that CK2 may control BRD4 phosphorylation to regulate fibrotic scar formation and affect outcomes after ischemic stroke. Our findings provide important insights into the role of CK2 in fibrotic scarring after cerebral ischemic injury and may open new avenues for stroke treatment. However, we will further investigate how p-BRD4 affects fibroblast activation and fibrotic scarring in vivo and in vitro.

Author Contributions Study conceptualization: XML, QY; methodology: XML, QHY, PRJ, JW, YC, JGH, MFT, JXR, QY; writing–original draft: XML, QHY, PRJ, JW; data curation: JW, YC, JGH, MFT; visualization: PRJ, JW, YC, JGH; writing–review and editing: XML; supervision: JW, YC, JGH, QY. All the authors have read and approved the final manuscript.

Data Availability The data supporting the findings are available from the corresponding author upon reasonable request.

Declarations

References

1. Gurtner GC, Werner S, Barrandon Y et al (2008) Wound repair and regeneration. Nature 453:314–321
2. Chew DJ, Fawcett JW, Andrews MR (2012) The challenges of long-distance axon regeneration in the injured CNS. Prog Brain Res 201:253–294
3. Hesp ZC, Yoseph RY, Suzuki R et al (2018) Proliferating NG2-cell-dependent angiogenesis and scar formation alter axon growth and functional recovery after spinal cord injury in mice. J Neurosci 38:1366–1382
4. Riew TR, Choi JH, Kim HL et al (2018) PDGFR-β-positive perivascular adventitial cells expressing nestin contribute to fibrotic scar formation in the striatum of 3-NP intoxicated rats. Front Mol Neurosci 11:402
5. Soderblom C, Luo X, Blumenthal E et al (2013) Perivascular fibroblasts form the fibrotic scar after contusive spinal cord injury. J Neurosci 33:13882–13887
6. Dias DO, Göritz C (2018) Fibrotic scarring following lesions to the central nervous system. Matrix Biol 68–69:561–570
7. D'Ambrosi N, Ambrosi N, Apolloni S (2020) Fibrotic scar in neurodegenerative diseases. Front Immunol 11:1394
8. Göritz C, Dias DO, Tomilin N et al (2011) A pericyte origin of spinal cord scar tissue. Science 333:238–242
9. Fernández-Klett F, Priller J (2014) The fibrotic scar in neurological disorders. Brain Pathol 24:404–413
10. Roth M, Enström A, Aghabeick C et al (2020) Parenchymal pericytes are not the major contributor of extracellular matrix in the fibrotic scar after stroke in male mice. J Neurosci Res 98:826–842
11. Dorrier CE, Aran D, Haenelt EA et al (2021) CNS fibroblasts form a fibrotic scar in response to immune cell infiltration. Nat Neurosci 24:234–244
12. Li Y, Chen Y, Tan L et al (2017) RNAi-mediated ephrin-B2 silencing attenuates astroglial-fibrotic scar formation and improves spinal cord axon growth. CNS Neurosci Ther 23:779–789
13. Zhu Y, Soderblom C, Krishnan V et al (2015) Hematogenous macrophage depletion reduces the fibrotic scar and increases axonal growth after spinal cord injury. Neurobiol Dis 74:114–125
14. Huang J, Chen Z, Li J et al (2017) Protein kinase CK2α catalytic subunit ameliorates diabetic renal inflammatory fibrosis via NF-κB signaling pathway. Biochem Pharmacol 132:102–117
15. Pinna LA (2002) Protein kinase CK2: a challenge to canons. J Cell Sci 115:3873–3878
16. Meggio F, Pinna LA (2003) One-thousand-and-one substrates of protein kinase CK2. FASEB J 17:349–368
17. Sajnaga E, Kubiński K, Szyszka R (2008) Catalytic activity of mutants of yeast protein kinase CK2alpha. Acta Biochim Pol 55:767–776
18. Sarno S, Reddy H, Meggio F et al (2001) Selectivity of 4,5,6,7-tetrabromobenzotriazole, an ATP site-directed inhibitor of protein kinase CK2 ('casein kinase-2'). FEBS Lett 496:44–48
19. Canton DA, Litchfield DW (2006) The shape of things to come: an emerging role for protein kinase CK2 in the regulation of cell morphology and the cytoskeleton. Cell Signal 18:267–275
20. Duncan JS, Litchfield DW (2008) Too much of a good thing: the role of protein kinase CK2 in tumorigenesis and prospects for therapeutic inhibition of CK2. Biochim Biophys Acta 1784:33–47
21. Singh NN, Ramji DP (2008) Protein kinase CK2, an important regulator of the inflammatory response. J Mol Med (Berl) 86:887–897
22. Zhang Q, Xia Y, Wang Y et al (2018) CK2 phosphorylating I2PP2A/SET mediates tau pathology and cognitive impairment. Front Mol Neurosci 11:146
23. Ampofo E, Nalbach L, Menger MD et al (2019) Protein kinase CK2-A putative target for the therapy of diabetes mellitus. Int J Mol Sci 20(18):4398
24. Zhang Y, Dees C, Beyer C et al (2015) Inhibition of casein kinase II reduces TGFβ induced fibroblast activation and ameliorates experimental fibrosis. Ann Rheum Dis 74:936–943
25. Li Y, Liu S, Han M et al (2017) NS5ATP13 promotes liver fibrogenesis via activation of hepatic stellate cells. J Cell Biochem 118:2463–2473
26. Ianni A, Hofmann M, Kumari P et al (2021) Depletion of numb and numblike in murine lung epithelial cells ameliorates bleomycin-induced lung fibrosis by inhibiting the β-catenin signaling pathway. Front Cell Dev Biol 9:639162
27. Sanz-Clemente A, Matta JA, Isaac JT et al (2010) Casein kinase 2 regulates the NR2 subunit composition of synaptic NMDA receptors. Neuron 67:984–996
28. Lussier MP, Gu X, Lu W et al (2014) Casein kinase 2 phosphorylates GluA1 and regulates its surface expression. Eur J Neurosci 39:1148–1158
29. Nguyen H, Zhu W, Baltan S (2022) Casein kinase 2 signaling in white matter stroke. Front Mol Biosci 9:908521
30. Kim GS, Jung JE, Niizuma K et al (2009) CK2 is a novel negative regulator of NADPH oxidase and a neuroprotectant in mice after cerebral ischemia. J Neurosci 29:14779–14789
31. Wen X, Klionsky DJ (2017) BRD4 is a newly characterized transcriptional regulator that represses autophagy and lysosomal function. Autophagy 13:1801–1803
32. Sanders YY, Lyv X, Zhou QJ et al (2020) Brd4-p300 inhibition downregulates Nox4 and accelerates lung fibrosis resolution in aged mice. JCI Insight 5(14):e137127
33. Gao J, Wei B, Liu M et al (2021) Endothelial p300 promotes portal hypertension and hepatic fibrosis through C-C motif chemokine ligand 2-mediated angiocrine signaling. Hepatology 73:2468–2483
34. Stratton MS, Haldar SM, McKinsey TA (2017) BRD4 inhibition for the treatment of pathological organ fibrosis. F1000Res 6:F1000
35. Cai X, Li Z, Zhang Q et al (2018) CXCL6-EGFR-induced Kupffer cells secrete TGF-β1 promoting hepatic stellate cell

activation via the SMAD2/BRD4/C-MYC/EZH2 pathway in liver fibrosis. J Cell Mol Med 22:5050–5061

36. Huang YH, Kuo HC, Yang YL et al (2019) MicroRNA-29a is a key regulon that regulates BRD4 and mitigates liver fibrosis in mice by inhibiting hepatic stellate cell activation. Int J Med Sci 16:212–220

37. Song S, Liu L, Yu Y et al (2019) Inhibition of BRD4 attenuates transverse aortic constriction- and TGF-β-induced endothelial-mesenchymal transition and cardiac fibrosis. J Mol Cell Cardiol 127:83–96

38. Segatto M, Szokoll R, Fittipaldi R et al (2020) BETs inhibition attenuates oxidative stress and preserves muscle integrity in Duchenne muscular dystrophy. Nat Commun 11:6108

39. Wilflingseder J, Willi M, Lee HK et al (2020) Enhancer and super-enhancer dynamics in repair after ischemic acute kidney injury. Nat Commun 11:3383

40. Chiang CM (2016) Phospho-BRD4: transcription plasticity and drug targeting. Drug Discov Today Technol 19:17–22

41. Wu SY, Nin DS, Lee AY et al (2016) BRD4 phosphorylation regulates HPV E2-mediated viral transcription, origin replication, and cellular MMP-9 expression. Cell Rep 16:1733–1748

42. Wu SY, Lee AY, Lai HT et al (2013) Phospho switch triggers Brd4 chromatin binding and activator recruitment for gene-specific targeting. Mol Cell 49:843–857

43. Iftner T, Haedicke-Jarboui J, Wu SY et al (2017) Involvement of Brd4 in different steps of the papillomavirus life cycle. Virus Res 231:76–82

44. Li X, Zhu H, Wen J et al (2022) Inhibition of BRD4 decreases fibrous scarring after ischemic stroke in rats by inhibiting the phosphorylation of Smad2/3. Brain Res 1797:148126

45. Percie du Sert N, Alfieri A, Allan SM et al (2017) The IMPROVE guidelines (Ischaemia models: procedural refinements of in vivo experiments). J Cereb Blood Flow Metab 37:3488–3517

46. Percie du Sert N, Hurst V, Ahluwalia A et al (2020) The ARRIVE guidelines 20: updated guidelines for reporting animal research. PLoS Biol 18:e3000410

47. Longa EZ, Weinstein PR, Carlson S et al (1989) Reversible middle cerebral artery occlusion without craniectomy in rats. Stroke 20:84–91

48. Kim S, Ham S, Yang K et al (2018) Protein kinase CK2 activation is required for transforming growth factor β-induced epithelial-mesenchymal transition. Mol Oncol 12:1811–1826

49. Wei J, Shan Y, Xiao Z et al (2022) Anp32e promotes renal interstitial fibrosis by upregulating the expression of fibrosis-related proteins. Int J Biol Sci 18:5897–5912

50. Hu B, Mao Z, Jiang X et al (2018) Role of TGF-β1/Smad3-mediated fibrosis in drug resistance mechanism of prolactinoma. Brain Res 1698:204–212

51. Gah A, Adil MS, Sabbineni H et al (2020) Differential regulation of TGFβ type-I receptor expressions in TGFβ1-induced myofibroblast differentiation. Can J Physiol Pharmacol 98:841–848

52. Chen Y, Huang J, Liu J et al (2023) Sirt1 overexpression inhibits fibrous scar formation and improves functional recovery after cerebral ischemic injury through the deacetylation of 14-3-3ζ. Mol Neurobiol 60:4795–4810

53. Canedo-Antelo M, Serrano MP, Manterola A et al (2018) Inhibition of casein kinase 2 protects oligodendrocytes from excitotoxicity by attenuating JNK/p53 signaling cascade. Front Mol Neurosci 11:333

54. Chen J, Li Y, Wang L et al (2001) Therapeutic benefit of intravenous administration of bone marrow stromal cells after cerebral ischemia in rats. Stroke 32:1005–1011

55. Bederson JB, Pitts LH, Tsuji M et al (1986) Rat middle cerebral artery occlusion: evaluation of the model and development of a neurologic examination. Stroke 17:472–476

56. Chiang T, Messing RO, Chou WH (2011) Mouse model of middle cerebral artery occlusion. J Vis Exp 48:2761

57. Huang JG, Ren JX, Chen Y et al (2023) M2 macrophages mediate fibrotic scar formation in the early stages after cerebral ischemia in rats. Neural Regen Res 18:2208–2218

58. Zhang Q, Soderland D, Steinle JJ (2014) TNFα inhibits IGFBP-3 through activation of p38α and casein kinase 2 in human retinal endothelial cells. PLoS ONE 9:e103578

59. Eom GH, Cho YK, Ko JH et al (2011) Casein kinase-2α1 induces hypertrophic response by phosphorylation of histone deacetylase 2 S394 and its activation in the heart. Circulation 123:2392–2403

60. Zdunek M, Silbiger S, Lei J et al (2001) Protein kinase CK2 mediates TGF-beta1-stimulated type IV collagen gene transcription and its reversal by estradiol. Kidney Int 60:2097–2108

61. Kim J, Hwan Kim S (2013) CK2 inhibitor CX-4945 blocks TGF-β1-induced epithelial-to-mesenchymal transition in A549 human lung adenocarcinoma cells. PLoS ONE 8(9):e74342

62. Calder J, Nagelberg A, Luu J et al (2021) Resistance to BET inhibitors in lung adenocarcinoma is mediated by casein kinase phosphorylation of BRD4. Oncogenesis 10(3):27

63. Shu S, Lin CY, He HH et al (2016) Response and resistance to BET bromodomain inhibitors in triple-negative breast cancer. Nature 529:413–417

64. Korb E, Herre M, Zucker-Scharff I et al (2015) BET protein Brd4 activates transcription in neurons and BET inhibitor Jq1 blocks memory in mice. Nat Neurosci 18:1464–1473

65. Liu S, Gao Y, Yu X et al (2016) Annexin-1 mediates microglial activation and migration via the CK2 pathway during oxygen-glucose deprivation/reperfusion. Int J Mol Sci 17(10):1770

66. Baltan S, Bastian C, Quinn J et al (2018) CK2 inhibition protects white matter from ischemic injury. Neurosci Lett 687:37–42

67. Bastian C, Quinn J, Tripathi A et al (2019) CK2 inhibition confers functional protection to young and aging axons against ischemia by differentially regulating the CDK5 and AKT signaling pathways. Neurobiol Dis 126:47–61

68. Münzer P, Walker-Allgaier B, Geue S et al (2017) CK2β regulates thrombopoiesis and Ca(2+)-triggered platelet activation in arterial thrombosis. Blood 130:2774–2785